npj | climate and atmospheric science

Article

Published in partnership with CECCR at King Abdulaziz University

https://doi.org/10.1038/s41612-024-00595-4

Quantifying sources of subseasonal prediction skill in CESM2

Jadwiga H. Richter[1] ✉, Anne A. Glanville[1], Teagan King[1], Sanjiv Kumar[2], Stephen G. Yeager[1], Nicholas A. Davis[3], Yanan Duan[2], Megan D. Fowler[1], Abby Jaye[4], Jim Edwards[1], Julie M. Caron[1], Paul A. Dirmeyer[5], Gokhan Danabasoglu[1] & Keith Oleson[1]

Subseasonal prediction fills the gap between weather forecasts and seasonal outlooks. There is evidence that predictability on subseasonal timescales comes from a combination of atmosphere, land, and ocean initial conditions. Predictability from the land is often attributed to slowly varying changes in soil moisture and snowpack, while predictability from the ocean is attributed to sources such as the El Niño Southern Oscillation. Here we use a set of subseasonal reforecast experiments with CESM2 to quantify the respective roles of atmosphere, land, and ocean initial conditions on subseasonal prediction skill over land. These reveal that the majority of prediction skill for global surface temperature in weeks 3–4 comes from the atmosphere, while ocean initial conditions become important after week 4, especially in the Tropics. In the CESM2 subseasonal prediction system, the land initial state does not contribute to surface temperature prediction skill in weeks 3–6 and climatological land conditions lead to higher skill, disagreeing with our current understanding. However, land-atmosphere coupling is important in week 1. Subseasonal precipitation prediction skill also comes primarily from the atmospheric initial condition, except for the Tropics, where after week 4 the ocean state is more important.

Subseasonal forecasts fill the gap between short-term weather forecasts that extend to 14 days and long-range seasonal outlooks that predict anomalous patterns several months ahead. Skillful forecasts on the subseasonal timescale are in high demand across multiple society-relevant sectors[1], however they are difficult to achieve and pose a frontier challenge in Earth system prediction[2]. In order to increase subseasonal prediction skill, the sources of subseasonal predictability on this timescale must be understood. While accurate atmosphere initial conditions (ICs) are of primary importance for skillful weather forecasts, predictability on the subseasonal timescale is believed to come from processes that evolve more slowly than the variability of the atmosphere, such as soil moisture and snowpack[2–4]. For example, anomalously dry soil can contribute to heat waves[5] and anomalously moist soil can contribute to persistent low temperature anomalies. The ocean state can also contribute to predictability, especially via coupled ocean-atmosphere modes of variability such as the El Niño Southern Oscillation (ENSO), the Madden–Julian Oscillation (MJO), and tropical-extratropical teleconnections[6,7]. There is evidence of a connection between ENSO and subseasonal prediction skill over the United States[8,9], and prediction of subseasonal variations of 2-m temperature anomalies over North America is improved during certain phases of the MJO[10,11].

Figure 1, adapted from a commonly shown graphic[12], illustrates the current hypothesis of the contributions of the atmosphere, land, and ocean to subseasonal prediction, assuming the ICs are a good approximation of the real world at that time. Specifically, the ICs would contain information about the background climatology plus coincident anomalies. The figure was originally developed by Paul Dirmeyer and is meant to be representative of a surface temperature forecast over land for a mid-continental location, like the central US, viewed as a combined initial-value problem for each of the three components. In such a location, the rapidly-decaying skill of the forecast on weather timescales (1 to 10 days) comes predominantly from the atmosphere. On monthly to seasonal timescales, the influence of remote ocean variability is thought to emerge as the main source of prediction skill. Predictability from the land initial state is hypothesized to be dominant between the weather and the seasonal timescale, with the importance of land

[1]Climate and Global Dynamics Laboratory, National Center for Atmospheric Research, Boulder, CO, USA. [2]College of Forestry, Wildlife, and Environment, Auburn University, Auburn, AL, USA. [3]Atmospheric Modeling and Chemistry Laboratory, National Center for Atmospheric Research, Boulder, CO, USA. [4]Mesoscale and Microscale Meteorology Laboratory, National Center for Atmospheric Research, Boulder, CO, USA. [5]Center for Ocean-Land-Atmosphere Studies, George Mason University, Fairfax, VA, USA. ✉e-mail: jrichter@ucar.edu

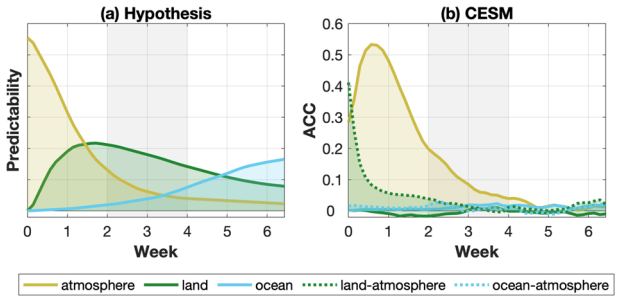

Fig. 1 | Sources of subseasonalpredictability of temperature. Predictability coming from the atmosphere (yellow), land (green), and ocean (blue) as a function of forecast time for annual mean 2 m temperature from 30°N to 60°N over land regions only: **a**) Hypothesis, adapted from a graphic by Paul Dirmeyer[7], (**b**) derived from CESM simulations Panel (b) includes additional two coupling terms: land-atmosphere (green dashed) and ocean-atmosphere (blue dashed). The derivation of (**b**) is described throughout the paper and further investigated in Fig. 4.

peaking around day 7 and slowly declining into the subseasonal window[13]. The National Oceanic and Atmospheric Administration (NOAA)'s Climate Prediction Center (CPC) subseasonal outlooks focus on the weeks 3–4 forecast. According to Fig. 1, in the weeks 3-4 forecast window, the land initial state is the largest source of predictability, with the ocean and atmosphere states having smaller, similarly sized contributions to predictability.

Despite the widespread acceptance of the graphic in Fig. 1, little research has been done to quantify the relative contributions of atmosphere, land, and ocean to predictability with the current generation of subseasonal prediction systems. Several studies have examined the contribution of land to subseasonal prediction skill. In particular, one study utilized the Global Land-Atmosphere Coupling Experiment (GLACE-2) consisting of coordinated experiments with and without realistic land surface initialization carried out by ten subseasonal forecast systems[14] and showed that realistic land had a notable positive impact on surface temperature prediction skill over North America out to 60 days, with the largest improvements of forecast skill for days 16–30 (r^2 increase of 0.05 to 0.1 for all dates, and up to 0.3 increase in some regions for extreme events). Some improvements were also noted for precipitation, however the impact was much smaller. The analysis of GLACE-2 was extended to all land areas in a subsequent study[15], which found soil moisture contributes to significant air temperature forecast skill. The impact of soil moisture on predictability as a function of time using the NOAA CFSv2 model was subsequently quantified[13]. The study showed that the land surface contributes to predictability the most between 5 days and 2 weeks, with a long tail of potential impacts stretching out to 2 months. A recent study found that the weeks 3–6 precipitation prediction skill over North America is primarily driven by sea-surface temperatures[16], implying that land and atmosphere instead have a very small contribution. Here we quantify the respective contributions of atmosphere, land, and ocean to subseasonal prediction skill over all land areas in the subseasonal prediction window, with a focus on surface temperature using a set of experiments with the Community Earth System Model, version 2 (CESM2) subseasonal prediction system.

Results

Surface temperature prediction skill

We quantify the respective contributions of atmosphere, land, and ocean to 2-meter temperature (2mT) prediction skill via reforecast experiments where the ICs of one or two model components are set to climatology (Table 1). By using climatological ICs for one component, we isolate the skill lost from not including the realistic state in that IC. Whereas, by using climatological ICs for two components, we estimate the skill gained from having a realistic state in the remaining component and its coupling with the other two components (see Table 1 and Calculations section). Figure 2 shows the annual 2mT anomaly correlation coefficient (ACC) for all the reforecast experiments. There are some seasonal variations in 2mT ACC, with the highest skill in December, January, February (DJF) and lower skill in June, July, August (JJA) (Supplementary Figs. 1 and 2). Annual values capture the most distinguishing features, though, and the seasonal variations over land areas are discussed in subsequent sections.

Consistent with findings from other subseasonal prediction systems[17], the standard forecasts show high ACC in weeks 1–2, a sharp decline into weeks 3–4, and a further minor decline into weeks 5–6 over the majority of land areas. The northern part of South America is the only land area that does not show a decrease of 2mT ACC from weeks 3–4 to weeks 5–6. Changing from realistic to climatological atmospheric ICs dramatically reduces the weeks 1–2 ACC over all land areas (Fig. 2d). Over the oceans, 2mT ACC is not impacted in the tropical eastern Pacific and Atlantic but is significantly smaller in the extratropics and western Pacific. The ACC remains lower for weeks 3-4 compared to the standard forecast, implying that the atmosphere contributes to prediction skill during this time period as well (Fig. 2e). This is confirmed by the complementary climoOCNclimoLND reforecast experiments (Fig. 2p, q), with realistic atmosphere ICs only, in which 2mT ACC over the majority of land areas and the Arctic Ocean is not significantly different from the standard reforecasts for weeks 1–2 and weeks 3–4.

At all lead times and over most regions, the change from realistic to climatological land ICs unexpectedly does not impact 2mT ACC, except for equatorial South America and Africa, Southeast Asia, and Siberia over which 2mT ACC increases (Fig. 2g, h, i). Many of the regions showing increased prediction skill with climatological land ICs are rainforests with high rainfall and taiga with permafrost, snow, and bogs, hence they have high levels of soil moisture year-round. In the absence of realistic atmosphere and oceanic ICs, the land ICs provide up to 30% of 2mT skill derived from the standard forecasts in weeks 1–2 as the land strongly couples with the atmosphere near the surface (Fig. 2s, t, u). In weeks 3–4 and weeks 5–6, the areas of skill from having realistic land ICs become sparse and largely overlap regions obtained from climatological initialization of all model components (Fig. 2m, n, o). The exceptions are northernmost South America and Australia where 2mT ACC is 0.2–0.3 in weeks 3–4 and weeks 5–6 (Fig. 2t, u). Overall, we find that in the absence of initializing the atmosphere, the surface air temperature over land will rapidly equilibrate with the realistic land surface and thereby gain some low-level predictive skill.

Initializing the ocean with climatological ICs results in a decrease in 2mT ACC over all oceans except the Arctic (Fig. 2 j, k, l). However, there is no statistically significant loss of skill over land in weeks 1–2, and little loss of skill in weeks 3–4 and weeks 5–6, excepting equatorial South America and Africa (Fig. 2 j, k, l) suggesting a rather small role of the ocean on the weeks 1–6 forecast. Teleconnections from oscillations such as ENSO and MJO in which the ocean plays a role are expected to be the strongest in DJF and are one of the reasons why 2mT ACC is expected to be higher in DJF. Indeed, there is an increase in 2mT ACC over equatorial South America and Africa, as well as the western United States in DJF and JJA, but those differences are rather small (Supplementary Figs. 2j, k, l and 2a, b, c). In the absence of realistic atmosphere and land ICs, realistic ocean ICs lead to small 2mT ACC (<0.2) in Weeks 1–4 over the majority of land areas (Fig. 2 v, w, x). In weeks 3–4 and weeks 5–6, the 2mT ACC over South America and central Africa is greater than that in the standard reforecasts, showing that ocean is the main source of prediction skill in those regions (Fig. 2v, w, x). The impact of the ocean on predictability in weeks 3–6 comes primarily from ENSO which is illustrated by an increase in ACC over South America, Africa, and the west coast of North America during active ENSO years (Fig. 3).

Quantification of sources of 2mT prediction skill

This set of reforecast experiments allows us to attribute subseasonal prediction skill due to the individual components and the coupling among them. From here onward, when we refer to skill from a coupled model component (atmosphere, land, or ocean), we are referring to the skill associated with that component's anomalies being present in the ICs. We

Table 1 | Summary of CESM2 reforecast experiments, including reforecast set name, designation of which model components have climatological and standard ICs, and sources of predictability

Reforecast Set	Climatological IC	Standard IC	Predictability Sources
standard	_____	atmosphere, land, & ocean	$Clim_{ALL}$, A_{ATM}, A_{LND}, A_{OCN}, C_{LNDATM}, C_{OCNATM}, C_{LNDOCN}
climoATM	atmosphere	land & ocean	$Clim_{ALL}$, A_{LND}, A_{OCN}, C_{LNDATM}, C_{OCNATM}, C_{LNDOCN}
climoLND	land	atmosphere & ocean	$Clim_{ALL}$, A_{ATM}, A_{OCN}, C_{LNDATM}, C_{OCNATM}, C_{LNDOCN}
climoOCN	ocean	atmosphere & land	$Clim_{ALL}$, A_{ATM}, A_{LND}, C_{LNDATM}, C_{OCNATM}, C_{LNDOCN}
climoOCNclimoLND[a]	ocean, land	atmosphere	$Clim_{ALL}$, A_{ATM}, C_{LNDATM}, C_{OCNATM}
climoATMclimoOCN	atmosphere, ocean	land	$Clim_{ALL}$, A_{LND}, C_{LNDATM}, C_{LNDOCN}
climoATMclimoLND	atmosphere, land	ocean	$Clim_{ALL}$, A_{OCN}, C_{OCNATM}, C_{LNDOCN}
climoALL	atmosphere, land, ocean	_____	$Clim_{ALL}$

Ocean here refers to ocean and sea-ice ICs. Predictability sources in the rightmost column include: climatology of atmosphere, land, and ocean initial states ($Clim_{ALL}$), atmosphere anomalies (A_{ATM}), land anomalies (A_{LND}), ocean anomalies (A_{OCN}), coupling between the land and atmosphere (C_{LNDATM}), coupling between the ocean and atmosphere (C_{OCNATM}), and coupling between the land and ocean (C_{LNDOCN}). When two model components are set to climatological ICs, we assume their coupling is close to zero.

[a]Due to limited computational resources, this set contains only 10 years of reforecasts for the months of April-October, and a full set for November-March. We have verified that a reduced time sample does not significantly change the results: it just makes them slightly noisier in the later weeks.

also derive skill gained from coupling between the model components by comparing experiments with realistic initialization of one and two model components (see Table 1 and Calculations section). Based on ACC averaged over global land, the largest contribution to 2mT prediction skill comes from atmosphere in weeks 1–4 (Fig. 4a). Beyond week 4, the ocean contributes most to 2mT prediction skill. In the CESM2 subseasonal prediction system, land does not contribute directly to prediction skill, however land-atmosphere coupling contributes during the first week of the forecast. As an example, if the observed land surface at initialization is colder than normal, it will draw the boundary layer toward colder than normal temperatures, regardless of whether the atmosphere is initialized with climatological or realistic conditions. In addition, ocean-atmosphere and land-atmosphere coupling also contribute to 2mT prediction skill throughout the forecast period at a level similar to that of the ocean.

The influence of land, atmosphere, and ocean on subseasonal prediction skill of 2mT varies as a function of latitude (Fig. 4b–d). In the Tropics (Fig. 4b), the role of the ocean is the largest, and prediction skill from the ocean and ocean-atmosphere coupling begins to exceed that from the atmosphere starting in week 3, most likely due to ENSO (Fig. 3). The role of land-atmosphere coupling in the Tropics is comparable to the role of the ocean for weeks 2–6. This is primarily true over South America likely due to the very large fraction of land coverage with vegetation (~90%) in that region[18]. In contrast to the Tropics, in mid and high latitudes, the prediction skill of 2mT comes primarily from the atmospheric initial conditions (Fig. 4c, d), with the ocean beginning to play a greater role only at week 5 of the forecast period.

For a direct comparison to Fig. 1a, b shows the CESM-derived schematic of sources of subseasonal predictability for annual mean 2m temperature for land regions averaged from 30°N to 60°N. The large role the atmosphere plays in the subseasonal window is similar between the hypothesis and CESM-based derivation. The role of land is strikingly different and needs future detailed exploration. The role of the ocean in CESM2-based prediction system is also lower than expected.

Linearity of the response

As shown by the reddish pink line and black line in Fig. 4, the ACC for the standard reforecast set and the sum of ACC for individual model components and coupling are approximately the same for the majority of the Earth's land surface, except for the Tropics. This implies that prediction skill is generally a linear combination of prediction skill from the atmosphere, ocean, and land, as well as atmosphere-land and ocean-atmosphere coupling, except for the Tropics where there is some redundancy from the coupling terms. For 2mT over land, effect of ocean-atmosphere coupling are small and land-atmosphere coupling is important during the first week of the forecast.

Sources of precipitation predictability

Subseasonal prediction skill of precipitation is about 4 to 5 times lower than that for 2mT[16,19,20]. Averaged over global land, the atmosphere is the dominant source of prediction skill for weeks 3–4 with the ocean and atmosphere playing approximately equal roles in weeks 5–6 (Fig. 4e). Similar to 2mT predictability, the land does not contribute much to prediction skill on the subseasonal timescale in CESM2, and the coupling terms are also small here. The prediction skill of precipitation varies with latitude. It is the largest in the Tropics and decreases with latitude (Fig. 4f–h). The atmosphere is the largest contributor to precipitation skill through week 3 in the Tropics, and the ocean becomes the dominant source of skill thereafter. This is primarily due to ENSO. During strong ENSO years, there is a 50–100% increase in precipitation prediction skill, primarily over South America and SE Asia/Australia in weeks 3–6, with the ocean being the dominant driver (not shown). In mid and high latitudes, the atmosphere is the primary source of precipitation predictability through week 3, with all terms being very small thereafter. Similar to 2mT, the ACC for the standard reforecast set and for sum of skill from individual model components and coupling are approximately the same for precipitation, with the coupling terms being fairly small.

Discussion

Using a set of experiments conducted with the CESM2 subseasonal prediction system we demonstrated that the atmosphere is the dominant source of subseasonal prediction skill of 2mT and precipitation over global land through week 3. In weeks 4 through 6, the role of the ocean is approximately equal to that of the atmosphere, except for the Tropics where the ocean is the dominant source of prediction skill. These results do not agree with the commonly accepted paradigm in which the role of land is much greater throughout the subseasonal window, and the ocean contribution is increasing from week 2 onward implying that either the commonly accepted paradigm needs adjustment or that the CESM2 based system is not capturing accurately some of the interactions between the Earth system model components The CESM2-based system has overall competitive subseasonal prediction skill[21]. Areas of improvement include addition of coupled data assimilation system and improved representation of coupling and feedback processes among various model components.

When interpreting these results it is important to keep in mind that the findings are representative of the entire 1999 to 2020 reforecast period as a whole, and that the role of predictive windows of opportunity such as ENSO and MJO are not explicitly displayed. By isolating active ENSO years we show that the role of the ocean on 2mT prediction skill is indeed larger during ENSO; However, it is still much smaller than what Fig. 1 suggests except in parts of South America and Africa. With the knowledge that CESM2 has a very good representation of ENSO teleconnections[22], these

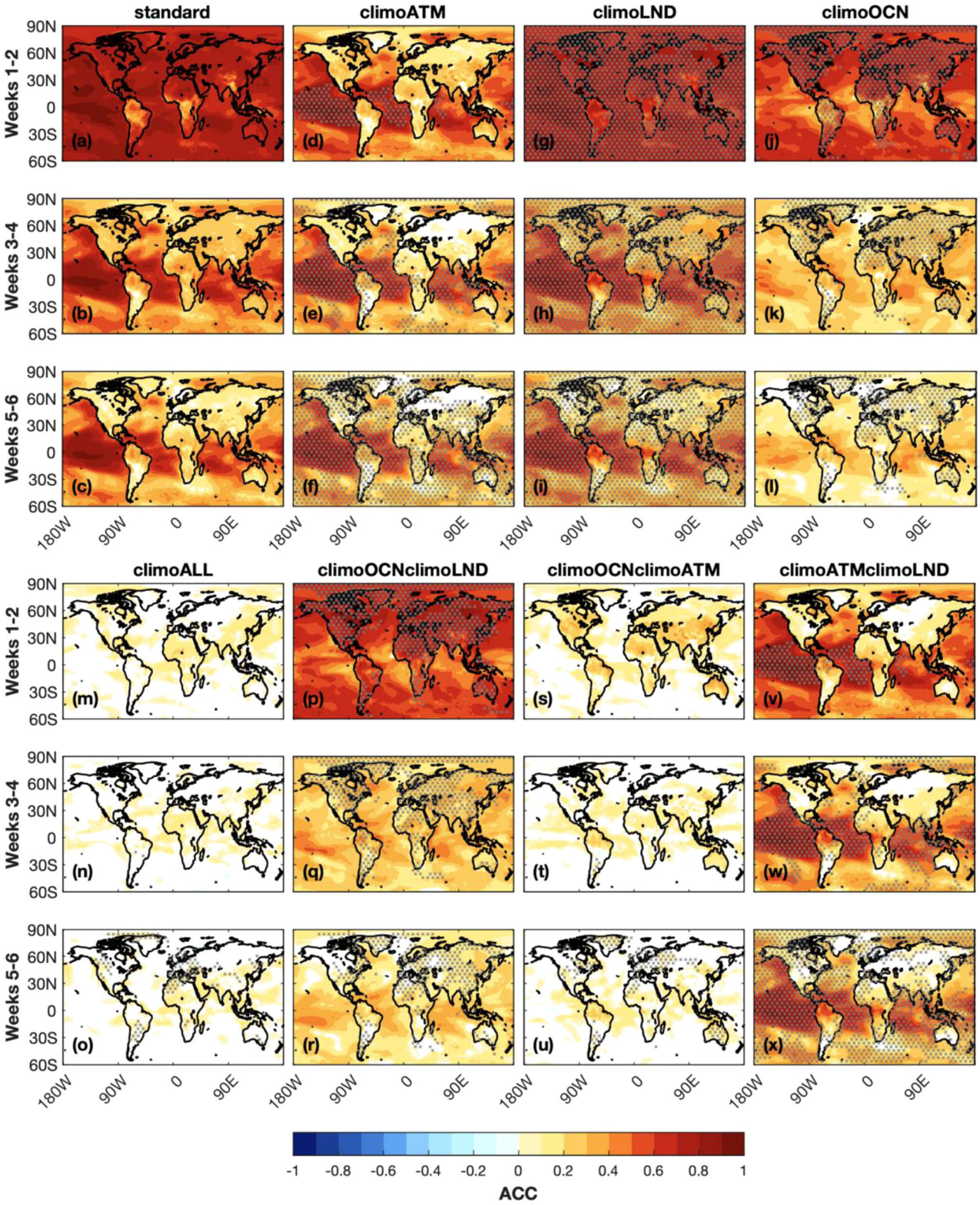

Fig. 2 | Prediction skill in CESM2reforecast experiments. Annual 2mT ACC for CESM2 over ocean and land for weeks 1–2 (**a**, **d**, **g**, **j**, **m**, **p**, **s**, **v**), weeks 3–4 (**b**, **e**, **h**, **k**, **n**, **q**, **t**, **w**), and weeks 5-6 (**c**, **f**, **i**, **l**, **o**, **r**, **u**, **x**) for standard reforecasts (**a**–**c**), climoATM (**d**–**f**), climoLND (**g**–**i**), climoOCN (**j**–**l**), climoALL (**m**–**o**), climoOCNclimoLND (**p**–**r**), climoOCNclimoATM (**s**–**u**), climoATMclimoLND (**v**–**x**). The white shading indicates regions not significantly different from zero according to a *t* test at the 95% confidence level. Areas of ACC in the experimental reforecast sets that are not statistically different from standard reforecasts are stippled.

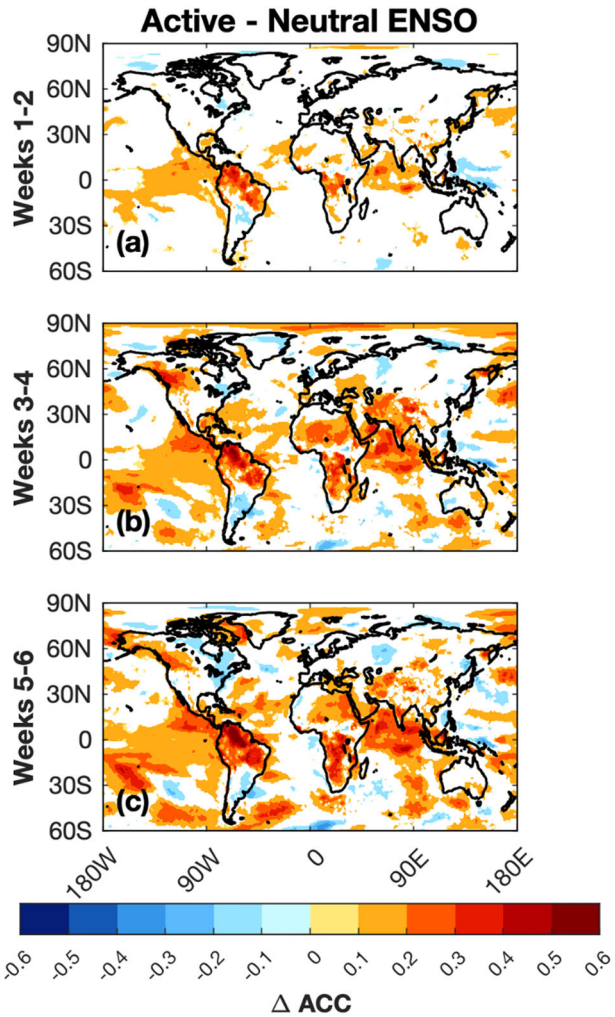

Fig. 3 | Role of ENSO. Difference of 2mT ACC for Active and Neutral ENSO states for the standard CESM2 reforecast set for (**a**) Weeks 1-2, (**b**) weeks 3-4, (**c**) weeks 5-6. Active ENSO states are defined as those forecasts that are initialized when the absolute value of SST anomalies averaged over the Nino 3.4 region are greater than 1 °C and neutral ENSO refers to absolute SST anomalies less than 0.5 °C at any time of the year. Findings are very similar for other reforecast sets with realistic ocean initialization (not shown). The white shading indicates regions not significantly different from zero according to a t-test at the 95% confidence level.

results imply that the role of the ocean on prediction skill is only beginning to grow in the subseasonal window and is not fully developed at these timescales, even when we look at active ENSO years. The quantification of the MJO and how it changes as a result of different initial conditions will be explored in future work.

In our modeling system, realistic land model initialization (including soil moisture) does not lead to improved prediction skill of 2mT or precipitation. Soil moisture initializations and its predictability are well represented in the CESM2 subseasonal prediction system given the initialization method used (Supplementary Fig. 3), however there still could be deficiencies in initial state representation due to lack of data assimilation. The standard reforecast experiment shows statistically significant soil moisture forecast skill in many land areas, including North America, Europe, Southeast Asia, and Australia. Soil moisture forecast skill is considerably higher in the standard reforecast experiment than the climoLND experiment, e.g., 50% higher for a point in the central US (bottom panel in Supplementary Fig. 3). However, we saw no increased temperature prediction skill in those places either. The high-latitude regions, e.g., including northern Canada, Alaska, northern and central Asia, and parts of Africa and South America, show minimal skill improvement due to soil moisture initialization. This result is partly related to data uncertainty issue, i.e., climate model-based soil moisture data, in this case, CESM2 subseasonal reforecast and ERA5-Land, agree well in the regions where a higher density of precipitation observation are found[15]. Additionally, we found a much higher soil moisture forecast skill by comparing the CESM2 subseasonal predictions with the corresponding land-only (CLM5) simulation driven by CFSR meteorological data (not shown).

We investigated further why the improved soil moisture forecast skills did not translate into the temperature prediction skill. The impact of soil moisture on surface temperature comes primarily via evaporation, with high soil moisture anomalies leading to increased evaporative cooling of the surface and negative surface air temperature anomalies, and vice versa for dry soils[23]. We found that the land surface air temperature and precipitation predictability was highest in areas with both strong soil moisture-evaporation coupling and long soil moisture memory[24]. Due to the differing strength of land-atmosphere coupling throughout the year, it was found that although soil moisture predictability was high over North America throughout spring and summer, atmosphere predictability was low in early spring and in fall due to low land-atmosphere coupling strength[24]. Capturing this atmosphere-land interaction in global models is dependent on a realistic representation of surface fluxes and their feedback on the atmosphere, which are difficult to validate as their observations are sparse. In order to understand the reason for why the land-atmosphere feedback in CESM2 is weak[25], and the contribution of the land initial state to prediction skill has not been realized, we have compared CESM2's terrestrial coupling index to available FLUXNET towers as well as to CESM1, a model that was closer to that used in the GLACE-2 study. Supplementary Figure 4 shows that in CESM2, strong and negative coupling is present between soil moisture and sensible heat flux in the summer hemispheres for each season. In DJF in the Southern Hemisphere, this is true in both CESM2 and CESM1, and is to some extent consistent with observations (particularly over Australia and South America). However, coupling in the Northern Hemisphere, while weaker than in the south, is stronger in CESM1 than in CESM2 Thus, it is likely that there is a weakened impact of soil moisture on surface fluxes in the boreal winter in CESM2. In JJA, there are also striking differences between CESM2 and CESM1. The latter indicated strong and negative coupling over almost all land regions, which would enable relatively stronger soil moisture-based modulation of surface fluxes than more modern versions of the model. Hence, overall our analysis suggests that land model changes that have occurred between CESM1 and CESM2 have reduced the strength of land-atmosphere coupling, especially in the Northern Hemisphere. Many of the model updates have occurred between the time of GLACE-2 and this particular study, making it somewhat unsurprising that our results may diverge from what has been established previously. The relatively weaker coupling could explain why the role of land initialization has a limited impact on subseasonal forecast skill, though this is a topic that deserves additional attention in the future. Future studies can explore the effects of land initialization on climate extremes, e.g., heat waves, where observation-based studies have found a critical role of land-atmosphere coupling[5,26]. A weak land-atmosphere coupling and/or lack of data assimilation could limit CESM's ability to capture these phenomena. As the findings of this study differ from the commonly accepted paradigm of the dominant sources of subseasonal predictability, it would be beneficial for similar studies to be carried out by other modeling centers to compare findings and for a focused effort to be carried out to improve land initialization and data assimilation, as well as to improve the representation of land-atmosphere coupling in Earth system models.

Methods

Forecasting system

We utilize the Community Earth System Model, version 2 (CESM2) subseasonal prediction system with the Community Atmosphere Model, version 6 (CAM6) as its atmospheric component[21]. The CESM2 subseasonal prediction system includes fully coupled atmosphere, ocean, land, sea-ice,

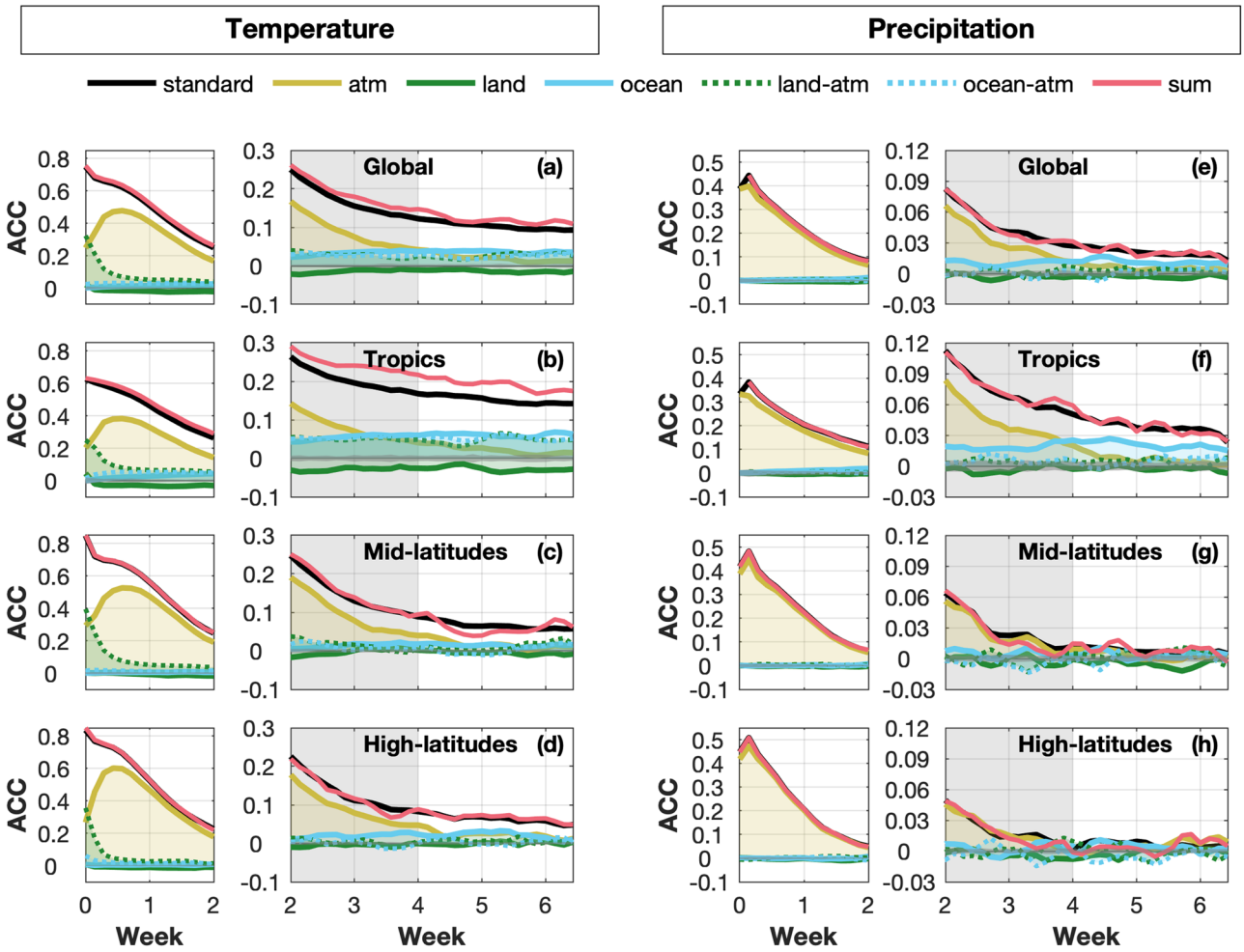

Fig. 4 | Sources of subseasonal predictability ofprecipitation. 2mT (two left columns) and precipitation (two right columns) ACC as a function of forecast lead time for the standard reforecast set (black) and attributed contributions of ACC from the atmosphere (yellow solid, AATM), land (green solid, ALND), and ocean (blue solid, AOCN). Contributions from land-atmosphere coupling (green dotted, C_{LNDATM}) and ocean-atmosphere coupling (blue dotted, C_{OCNATM}) are also shown. Sum (pinkish red) is the total of these components. Averages over global land are shown in panels (**a**) and (**e**), Tropics (30°S - 30°N) in (**b**) and (**f**), Mid-latitudes (30°N - 60°N and 30°S - 60°S) in (**c**) and (**g**), and High-Latitudes (60°N to 90°N and 60°S to 90°S) in (**d**) and (**h**). Light gray shading highlights the weeks 3–4 forecast window. Note that the first two weeks are missing from the labeled precipitation figures to highlight the subseasonal window. The entire forecast period for precipitation is shown in the top right panel for global land.

river, and wave models with approximate 1° horizontal resolution in all components[27]. Standard CESM2 reforecasts are initialized weekly from 1999 to 2020. Reforecasts are 45 days long with an 11-member ensemble. The atmosphere model is initialized using the National Centers for Environmental Prediction (NCEP) CFSv2 reanalysis[28,29] interpolated to the CAM6 grid. Land ICs for CESM2 reforecasts come from a stand-alone Community Land Model, version 5 (CLM5) simulation forced by CFSv2 reanalysis[21]. Ocean and sea-ice ICs are obtained from a stand-alone ocean sea-ice coupled configuration of CESM2 forced with the adjusted Japanese 55-year reanalysis product state fields and fluxes (JRA55-do forcing[29]). Ensemble spread is generated using a random field perturbation method[21,30,31].

The realism of land model initialization has been verified by comparing root zone soil moisture (0–0.5 m) forecast with the ERA5-Land observation[32](Supplementary Fig. 3). Snow-pack initialization, which affects primarily high-latitudes in boreal winter was also compared to observation. In agreement with other Earth system models participating in phase 6 of the Coupled Model Intercomparison Project, CESM2 overestimates the snow water equivalent in high-latitudes[33] however the seasonal cycle, location, and inter-annual variability is in good agreement with the observations (Supplementary Fig. 5). The sea surface temperatures (SSTs) from JRA55-do forced ocean simulation used to initialize the reforecasts correlate very highly with the Hadley Centre Sea Ice and Sea Surface Temperature dataset[5] (HadISST[34]). Specifically, correlations between the simulation and HadISST were found to be close to 1 over the majority of ocean basins, with smaller values in the Arctic Ocean and near the maritime continent. JRA55-do forced ocean simulation also tracks the observed ENSO index very closely[21].

Subseasonal forecasting skill of key quantities was evaluated[21] showing that the CESM2 subseasonal prediction system has surface temperature and precipitation skill comparable to the National Oceanic and Atmospheric Administration (NOAA) CFSv2 model, but slightly lower than that of the European Centre for Medium-Range Weather Forecasts (ECMWF) model. It was also shown that the MJO in CESM2 is predictable out to ~25 days, a few days longer than in the NOAA CFSv2 system, but slightly less than that in the ECMWF system[21]. The CESM2 subseasonal prediction system exhibits a small initialization shock during the first day of the forecast due to the initialization methods and lack of data assimilation, which could contribute to spurious results during the first few days of the forecast. Although the CESM-based prediction systems do not use data assimilation in model initialization, the subseasonal prediction skill is equal to or higher than other SubX models, several of which do use data assimilation, as shown for CESM1-based system[30].

Experiments

We carry out seven additional subseasonal reforecast sets following the same reforecast protocol as for the standard reforecasts but with climatological ICs for one or more of the model components as described in Table 1. For example, the climoATM reforecast set uses climatological atmosphere ICs in conjunction with land and ocean ICs from the standard set. Climatological atmosphere ICs for every day of the year were created from the CFSv2 daily reanalysis for the time period from 1999 to 2020. Climatological ocean ICs were created in a similar manner by averaging the daily ICs from the default forecasts. Due to discontinuities in sea-ice from year to year, the simple averaging procedure did not work for creating the sea-ice climatology, hence 2010 conditions were chosen as a neutral year, in the middle of the reforecast period, instead of climatology for sea-ice in the climoOCN runs. To create land ICs, we spun up CLM5 in a stand-alone mode, forced by the NCEP CFSv2 atmospheric datasets from 1979 to 1984. This 6-year segment was cycled 115 times until a quasi-equilibrium state was achieved. Thus, this spin-up run was integrated for 690 years. To obtain the standard land ICs, we started from the end of the spin-up run and integrated forward from 1979 through 2020, using the standard NCEP CFSv2 atmospheric datasets as the forcing. For the climatological land ICs, we again started from the end of the spin-up run and performed an additional 210-year integration using climatological annual-cycle NCEP CFSv2 atmospheric datasets averaged for the 1979–2020 period. At the end of this simulation, we verified that a quasi-equilibrium climatological state was achieved for certain variables of interest, such as total leaf area index and soil moisture. The final state of this simulation was then used as the climatological IC for land (e.g., Supplementary Fig. 3e).

Verification Datasets

The ECMWF Reanalysis v5 (ERA5) is used for 2mT verification to include global ocean and land coverage. We use daily mean 2mT output and interpolate it onto a 1°x 1° grid to match the post-processed format of the CESM2 reforecast output. The Global Precipitation Climatology Project (GPCP)[35] dataset is used for precipitation verification, and it is also interpolated. Calculations were repeated using the NOAA Climate Prediction Center (CPC) Global Daily Temperature and Gauge-Based Precipitation[36] datasets, which yield very similar results over land. Finally, we used ERA5-Land[31] data for soil moisture and snow water equivalent verification.

Calculations

We calculate global ACC for temperature and precipitation using anomalies relative to a lead dependent climatology, following the methodology described by ref. 19. We use the resulting ACC to define the prediction skill for various model components over different land regions. For time-varying ACC figures (Fig. 4), ACC is calculated daily and subsequently averaged over the globe and various latitude bands (over land only). For precipitation, a 3-day moving average is applied to reduce noise.

By using ACC to define prediction skill in our reforecast sets, we can also use it to deduce skill in individual components. In order to derive contributions from the atmosphere, land, and ocean, we assume that the ACC from the standard reforecast set is equal to a linear sum of ACC from climatology ($Clim_{ALL}$), anomalies in the three model components (A_{ATM}, A_{LND}, and A_{OCN}), and coupling between components (C_{LNDATM}, C_{OCNATM}, and C_{LNDOCN}). By using climatological conditions for certain model components in our experimental reforecast sets, we create ICs that lack anomalies and coupling interactions between certain model components. By calculating ACC in these various simulations, we can derive ACC associated with individual components, and derive the coupling terms by comparing the various simulations. We define coupling as interactions or adjustments that take place between two components. Coupling will be small when model components are in balance and larger when they are not. For example, land-atmosphere coupling (C_{LNDATM}) will be small when the atmosphere and land are both set to climatology, and it will be larger when one is out of balance.

The ACC derived from the standard forecast is a combination of ACC from climatology, anomalies, and coupling. Speaking in terms of ACC, we can define:

$$\mathbf{standard} = Clim_{ALL} + A_{ATM} + A_{LND} + A_{OCN} + C_{LNDATM} + C_{OCNATM} + C_{LNDOCN} \quad (1)$$

where bolding indicates that the quantity is directly derived from a given reforecast set. When climatological initial conditions are used for a single component, that component's anomaly term no longer contributes to the ACC, and the ACC for those reforecasts sets comes from fewer terms:

$$\mathbf{climoATM} = Clim_{ALL} + A_{LND} + A_{OCN} + C_{LNDATM} + C_{OCNATM} + C_{LNDOCN} \quad (2)$$

$$\mathbf{climoLND} = Clim_{ALL} + A_{ATM} + A_{OCN} + C_{LNDATM} + C_{OCNATM} + C_{LNDOCN} \quad (3)$$

$$\mathbf{climoOCN} = Clim_{ALL} + A_{ATM} + A_{LND} + C_{LNDATM} + C_{OCNATM} + C_{LNDOCN} \quad (4)$$

The above assumes that the average coupling between the various components does not change much between the reforecast sets. For example, we expect the coupling between the atmosphere and land in the **standard** reforecast set to be similar to the atmosphere and land coupling in the **climoATM** reforecast set.

We can solve for the ACC associated with atmospheric anomalies (A_{ATM}) by subtracting Eq. (2) from Eq. (1). We can also calculate the ACC associated with land (A_{LND}) and ocean (A_{OCN}) anomalies in a similar fashion, hence:

$$(Clim_{ALL} + A_{ATM} + A_{LND} + A_{OCN} + C_{LNDATM} + C_{OCNATM} + C_{LNDOCN}) - (Clim_{ALL} + A_{LND} + A_{OCN} + C_{LNDATM} + C_{OCNATM} + C_{LNDOCN}) = A_{ATM} \quad (5)$$

$$(Clim_{ALL} + A_{ATM} + A_{LND} + A_{OCN} + C_{LNDATM} + C_{OCNATM} + C_{LNDOCN}) - (Clim_{ALL} + A_{ATM} + A_{OCN} + C_{LNDATM} + C_{OCNATM} + C_{LNDOCN}) = A_{LND} \quad (6)$$

$$(Clim_{ALL} + A_{ATM} + A_{LND} + A_{OCN} + C_{LNDATM} + C_{OCNATM} + C_{LNDOCN}) - (Clim_{ALL} + A_{ATM} + A_{LND} + C_{LNDATM} + C_{OCNATM} + C_{LNDOCN}) = A_{OCN} \quad (7)$$

When climatological initial conditions are used for two components, we assume their two anomaly terms are negligible, along with their shared coupling term, and the ACC for those sets is as follows:

$$\mathbf{climoOCNclimoLND} = Clim_{ALL} + A_{ATM} + C_{LNDATM} + C_{OCNATM} \quad (8)$$

$$\mathbf{climoOCNclimoATM} = Clim_{ALL} + A_{LND} + C_{LNDATM} + C_{LNDOCN} \quad (9)$$

$$\mathbf{climoATMclimoLND} = Clim_{ALL} + A_{OCN} + C_{OCNATM} + C_{LNDOCN} \quad (10)$$

The ACC from climatology ($Clim_{ALL}$) is derived from the climoALL suite, or simply:

$$\mathbf{climo_{ALL}} = Clim_{ALL} \quad (11)$$

By subtracting Eq. (11) from Eqs. (8) through (10) we can deduce the anomalies and coupling terms associated with each component:

$$(Clim_{ALL} + A_{ATM} + C_{LNDATM} + C_{OCNATM} - (Clim_{ALL}) = A_{ATM} + C_{LNDATM} + C_{OCNATM} \quad (12)$$

$$(\mathrm{Clim_{ALL}} + \mathrm{A_{LND}} + \mathrm{C_{LNDATM}} + \mathrm{C_{LNDOCN}}) - (\mathrm{Clim_{ALL}}) = \mathrm{A_{LND}} + \mathrm{C_{LNDATM}} + \mathrm{C_{LNDOCN}} \quad (13)$$

$$(\mathrm{Clim_{ALL}} + \mathrm{A_{OCN}} + \mathrm{C_{OCNATM}} + \mathrm{C_{LNDOCN}}) - (\mathrm{Clim_{ALL}}) = \mathrm{A_{OCN}} + \mathrm{C_{OCNATM}} + \mathrm{C_{LNDOCN}} \quad (14)$$

Assuming that the land-ocean coupling (C_{LNDOCN}) is nearly zero over land, we can then use A_{LND} and A_{OCN}, (from Eqs. 6 and 7) to solve for C_{LNDATM} and C_{OCNATM} in the right-hand side of Eqs. (13) and (14), respectively. If the linearity assumption holds, we should be able to arrive at the standard ACC by adding the ACC from individual model components:

$$\mathrm{sum} = \mathrm{Clim_{ALL}} + \mathrm{A_{ATM}} + \mathrm{A_{LND}} + \mathrm{A_{OCN}} + \mathrm{C_{LNDATM}} + \mathrm{C_{OCNATM}} \quad (15)$$

Figure 4 shows us that this assumption is valid.

In addition to ACC, we have calculated the Ranked Probability Skill Score (RPSS) for all the simulations presented here. The changes in RPSS between various simulation reflect the sane key findings of our study based on the ACC calculations, and are not shown.

Data availability

GPCP data and the ERA5 Reanalysis are available freely from the NCAR/UCAR Research Archive at https://rda.ucar.edu/datasets/. All CESM2 reforecast sets are available on the NCAR Climate Data Gateway at https://doi.org/10.5065/0s63-m767.

Code availability

All CESM2 simulations were carried out with CESM tag: cesm2.1 which is freely available from https://github.com/ESCOMP/CESM/tree/cesm2.1_s2sfcst1.0. Calculation and plotting scripts are available from https://doi.org/10.5281/zenodo.7926660.

Received: 7 July 2023; Accepted: 15 February 2024;
Published online: 04 March 2024

References

1. White, C. J. et al. Potential applications of subseasonal-to-seasonal (s2s) predictions. *Met. Appl.* **24**, 315–325 (2017).
2. National Academies of Sciences, Engineering, and Medicine. *Next Generation Earth System Prediction: Strategies for Subseasonal to Seasonal Forecasts*, Washington, DC: The National Academies Press (2016). https://doi.org/10.17226/21873. https://nap.nationalacademies.org/catalog/21873/next-generation-earth-system-prediction-strategies-for-subseasonal-to-seasonal#:~:text=Next%20Generation%20Earth%20System%20Predictions,medium%20and%20extended%20lead%20times.
3. Koster, R. D. & Suarez, M. J. Soil moisture memory in climate models. *J. Hydrometeorol.* **2**, 558–570 (2001).
4. Dirmeyer, P. A., Schlosser, C. A. & Brubaker, K. L. Precipitation, recycling, and land memory: an integrated analysis. *J. Hydrometeorol.* **10**, 278–288 (2009).
5. Miralles, D. et al. Mega-heatwave temperatures due to combined soil desiccation and atmospheric heat accumulation. *Nat. Geosci.* **7**, 345–349 (2014).
6. Vitart, F. Robertson A. W. and the S2S steering group. Sub-seasonal to seasonal prediction: linking weather and climate. Seamless prediction of the earth system: from minutes to months, G. Brunet, S. Jones, and P. M. Ruti, Eds., WMO-1156, World Meteorological Organization, **1156**, 385–401 (2015). http://library.wmo.int/pmb_ged/wmo_1156_en.pdf.
7. Mariotti, A. et al. Windows of opportunity for skillful forecasts subseasonal to seasonal and beyond. *Bull. Am. Meteor. Soc.* **101**, E608–E625 (2020).
8. DelSole, T., Trenary, L., Tippett, M. K. & Pegion, K. Predictability of week-3–4 average temperature and precipitation over the contiguous United States. *J. Clim.* **30**, 3499–3512 (2017).
9. Wang, L. & Robertson, A. W. Week 3–4 predictability over the United States assessed from two operational ensemble prediction systems. *Clim. Dyn.* **52**, 5861–5875 (2019).
10. Zhou, S., L'Heureux, M., Weaver, S. & Kumar, A. A composite study of the MJO influence on the surface air temperature and precipitation over the Continental United States. *Clim. Dyn.* **38**, 1459–1471 (2012).
11. Rodney, M., Lin, H. & Derome, J. Subseasonal prediction of wintertime North American surface air temperature during strong MJO events. *Mon. Wea. Rev.* **141**, 2897–2909 (2013).
12. Mariotti, A., Ruti, P. M. & Rixen, M. Progress in subseasonal to seasonal prediction through a joint weather and climate community effort. *npj Clim. Atmos. Sci.* **1**, 4 (2018).
13. Dirmeyer, P. A., Halder, S. & Bombardi, R. On the harvest of predictability from land states in a global forecast model. *J. Geophys. Res. Atmos.* **123**, 13111–13127 (2018).
14. Koster, R. D. et al. Contribution of land surface initialization to subseasonal forecast skill: first results from a multi-model experiment. *Geophys. Res. Lett.* **37**, L02402 (2010).
15. Koster, R. D. et al. The second phase of the global land–atmosphere coupling experiment: soil moisture contributions to subseasonal forecast skill. *J. Hydrometeorol.* **12**, 805–822 (2011).
16. Sun, L. et al. Attribution of North American subseasonal precipitation prediction skill. *Wea. Forecast.* **37**, 2069–2085 (2022).
17. Pegion, K. et al. The subseasonal experiment (SubX): a multimodal subseasonal prediction experiment. *Bull. Am. Meteor. Soc.* **100**, 2043–2060 (2019).
18. Dirmeyer, P. A. et al. Model estimates of land-driven predictability in a changing climate from CCSM4. *J. Clim.* **26**, 8495–8512 (2013).
19. Vitart, F. Evolution of ECMWF sub-seasonal forecast skill scores. *Q. J. R. Meteorol. Soc.* **140**, 1889–1899 (2014).
20. Wang, S., Anichowski, A., Tippett, M. K. & Sobel, A. H. Seasonal noise versus subseasonal signal: forecasts of California precipitation during the unusual winters of 2015–2016 and 2016–2017. *Geophys. Res. Lett.* **44**, 9513–9520 (2017).
21. Richter, J. H. et al. Subseasonal earth system prediction with CESM2. *Wea. Forecast.* **37**, 797–815 (2022).
22. Fasullo, J. T. Evaluating simulated climate patterns from the CMIP archives using satellite and reanalysis datasets using the Climate Model Assessment Tool (CMATv1). *Geosci. Model Dev.* **13**, 3627–3642 (2020).
23. Fischer, E. M., Seneviratne, S. I., Lüthi, D. & Schär, C. Contribution of land-atmosphere coupling to recent European summer heat waves. *Geophys. Res. Lett.* **34**, L06707 (2007).
24. Guo, Z., Dirmeyer, P. A. & DelSole, T. Land surface impacts on subseasonal and seasonal predictability. *Geophys. Res. Lett.* **38**, L24812 (2011).
25. Mei, R. & Wang, G. Summer land–atmosphere coupling strength in the United States: Comparison among observations, reanalysis data, and numerical models. *J. Hydrometeorol.* **13**, 1010–1022 (2012).
26. Dirmeyer, P. A., Balsamo, G., Blyth, E. M., Morrison, R. & Cooper, H. M. Land-atmosphere interactions exacerbated the drought and heatwave over northern Europe during summer 2018. *AGU Adv.* **2**, e2020AV000283 (2001).
27. Danabasoglu, G. et al. The Community Earth System Model Version 2 (CESM2). *J. Adv. Model. Earth Syst.* **12**, e2019MS001916 (2020).
28. Saha, S. et al. The NCEP climate forecast system version 2. *J. Clim.* **27**, 2185–2208 (2014).
29. Tsujino, H. et al. JRA-55 based surface dataset for driving ocean–sea-ice models (JRA55-do). *Ocean Model.* **130**, 79–139 (2018).
30. Magnusson, L., Nycander, J. & Kallen, E. Flow-dependent versus flow-independent initial perturbations for ensemble prediction. *Tellus* **61A**, 194–209 (2009).

31. Richter, J. H. et al. Subseasonal prediction with and without a well-represented stratosphere in CESM1. *Wea. Forecast.* **35**, 2589–2602 (2020).
32. Muñoz-Sabater, J. et al. ERA5-Land: a state-of-the-art global reanalysis dataset for land applications. *Earth Syst. Sci. Data* **13**, 4349–4383 (2021).
33. Kouki, K. et al. Evaluation of Northern Hemisphere snow water equivalent in CMIP6 models during 1982–2014. *Cryosphere* **16**, 1007–1030 (2022).
34. Rayner, N. A. et al. Global analyses of sea surface temperature, sea ice, and night marine air temperature since the late nineteenth century. *J. Geophys. Res.* **108**, 4407 (2003).
35. Adler, R. F. et al. The Global Precipitation Climatology Project (GPCP) Monthly Analysis (New Version 2.3) and a Review of 2017 Global Precipitation. *Atmosphere* **9**, 138 (2018).
36. Chen, M. et al. Assessing objective techniques for gauge-based analyses of global daily precipitation. *J. Geophys. Res.* **113**, D04110 (2008).

Acknowledgements

This work was supported by the National Center for Atmospheric Research (NCAR), which is a major facility sponsored by the National Science Foundation (NSF) under Cooperative Agreement 1852977. Portions of this study were supported by the Regional and Global Model Analysis (RGMA) component of the Earth and Environmental System Modeling Program of the U.S. Department of Energy's Office of Biological and Environmental Research (BER) via NSF Interagency Agreement 1844590. Computing and data storage resources, including the Cheyenne Supercomputer (https://doi.org/10.5065/D6RX99HX), were provided by the Computational and Information Systems Laboratory (CISL) at NCAR. SK and YD acknowledge the support of USDA grant # 2020-67021-32476. We thank Monastir Maruf (Ph.D. student, Auburn University) for running CLM offline with CFSR meteorological forcing data for comparison with ERA5 Land soil moisture data, and Judith Berner for comments that helped to improve the manuscript.

Author contributions

J.R. led the study, produced ICs, ran simulations, and led the write-up. A.G. did majority of the analysis, produced ICs, archived simulations, T.K. ran simulations, M.F. and A.J. contributed to analysis, J.C. produced ICs, Y.D. and S.K. analyzed land ICs. A.G., S.K., N.D., P.D., S.Y., G.D. provided valuable input into the study design and interpretation. All authors contributed to the writing of the manuscript.

Competing interests

The authors declare no competing interests.

Additional information

Supplementary information The online version contains supplementary material available at https://doi.org/10.1038/s41612-024-00595-4.

Correspondence and requests for materials should be addressed to Jadwiga H. Richter.